Theoretical and Applied Fracture Mechanics 121 (2022) 103434

Contents lists available at ScienceDirect

Theoretical and Applied Fracture Mechanics

journal homepage: www.elsevier.com/locate/tafmec

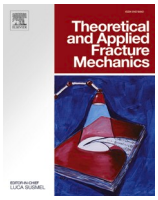

Effect of strain rate on tensile fracture behavior of notched polyamide 12 processed by selective laser sintering

T. Gómez-del Río [a,*], M. Crespo [a], R. López [b], J. Rodríguez [a]

[a] DIMME, Grupo de Durabilidad e Integridad Mecánica de Materiales Estructurales, Universidad Rey Juan Carlos, Escuela Superior de Ciencias Experimentales y Tecnología, C/ Tulipán, s/n. Móstoles, 28933 Madrid, España
[b] Departamento de Optoelectrónica y Misilística. Campus "La Marañosa", Instituto Nacional de Técnica Aeroespacial (INTA), Ctra. M301 km 10.5, 28330 San Martín de la Vega, España

ARTICLE INFO

Keywords:
Polyamide
Notched sample
Additive manufacturing
Strain rate
Theory of critical distances

ABSTRACT

In this work, the applicability of the Theory of Critical Distances to the study of failure at high-loadings rates of polyamide 12 notched specimens additively manufactured by selective laser sintering, is evaluated. An experimental and numerical study has been carried out and values of modulus of elasticity, tensile strength and fracture toughness have been obtained. under static and dynamic conditions. The effect of orientation has also been analyzed, testing samples parallel and perpendicular to the layers of material deposited.

1. Introduction

The great sensitivity of polymers to strain rate is a well-known fact in the scientific community. Significant changes in the elastic modulus and yield stress occur when the strain rate varies by several orders of magnitude [1]. Very interesting results have been published on polycarbonate [2], polypropylenes [3], polyamides [4] and epoxy resins [5,6]. Thermally activated models are the most widely used to describe this strain rate dependence [7]. Their results are acceptable for moderate strain rate variations, although in case of reaching very high rates, such as those characteristics in impact tests (Hopkinson bar and similar ones at the laboratory level), models must be modified [2,8].

The most commonly used materials for 3D printing are thermoplastic polymers. Polyamides (particularly PA12) are one of the most widely used families in additive manufacturing, both for their thermal properties that facilitate the manufacturing process and for the final mechanical properties obtained [9–10]. Additive manufactured polyamides can be found in different applications in very diverse fields, from automotive or aeronautics to biomedical or defence engineering [11–13].

Due to the relative novelty in the use of components manufactured by additive techniques, a great research effort is required on the mechanical behaviour of these materials and components [14–19]. In layer-by-layer additive manufacturing processes, a series of characteristic defects appear, such as non-melted particles or porosity, which can affect the mechanical response and integrity of the components thus manufactured. Fracture behaviour is especially sensitive to the defect population and must be considered in any analysis of structural integrity [20–22].

The analysis of notched samples is essential in structural mechanics since many components contain notches, making it necessary to have an adequate theory for their study. Direct application of fracture mechanics to notched components, considering the notches as cracks, leads to poor predictions. Therefore, methodologies that consider the real behaviour of the notches are needed. In this sense, the pioneering work of Neuber [23] and the investigations of Lazzarin and coworkers about the stress fields around notches should be recognized. [24–26]. Different works have been published in the context of notch fracture mechanics using different methodologies: the strain energy density [27], the cohesive zone model [28] or the Theory of Critical Distances (TCD) [29–30].

The TCD and its different approaches can be applied to the analysis of the load capacity of components that contain any type of stress risers, from plain samples (without stress concentrations) to cracked components, passing through any other type of defects, such as notches, holes and pores [31–32].

The TCD is a group of methodologies that allows the estimation of failure loads of notched components by considering linear-elastic stress fields in the vicinity of the stress concentrators. All these methods rely on a characteristic material length, L, that can be determined through the following equation:

* Corresponding author.
E-mail address: mariateresa.gomez@urjc.es (T. Gómez-del Río).

https://doi.org/10.1016/j.tafmec.2022.103434
Received 8 March 2022; Received in revised form 3 June 2022; Accepted 6 June 2022
Available online 16 June 2022

$$L = \frac{1}{\pi}\left(\frac{K_{IC}}{\sigma_0}\right)^2 \quad (1)$$

where k_{IC} is the fracture toughness of the material and σ_0 is the inherent material stress [33–35]. Both, L and σ_0 can be determined through experimental tests using components with different geometries and finding the intersection between their stress-distance curves, as showed in Fig. 1.

There are different approaches in the TCD to predict the failure, including the point method (PM), line method (LM), the area method (AM) and the volume method (VM). In the present work, the procedure used to apply the TCD has been the PM (Fig. 1), which establishes as a failure criterion that the stress evaluated along the tip of the notch at a distance of L/2 reaches the value of σ0. Such a condition can be expressed by the following equation:

$$\sigma_\theta\left(\theta = 0, r = \frac{L}{2}\right) = \sigma_0 \quad (2)$$

The application of the TCD to notched polymers has specific characteristics that distinguish them from other materials. It has been known for a long time that the inherent material stress does not coincide with the yield stress but must normally has to values several times higher to make more accurate predictions [36]. As mentioned above, strain rate is one of the variables with high influence on the mechanical behaviour of polymers and its effect should not be ignored. Failure criteria of notched samples should also consider this strain rate dependence. For example, in the TCD the inherent material stress should increase with strain rate in the same way the yield stress does. Therefore, a material characterisation is needed.

Few works have attempted to include the influence of strain rate on the TCD parameters. To the authors' knowledge, this has been done on a few occasions, including the work of Yin et al. in metals [37] and some preliminary results published by the authors on the influence of the strain rate on the TDC parameters in polyamide 12 [38]. This work is a continuation of that one in which the determination of the fracture toughness at different strain rates is also addressed.

Thus, the objective of this work is to provide validation on the application of the TCD to the analysis of the notch effect on Polyamide 12 manufactured by SLS, taking into consideration the orientation (possible anisotropic behaviour) and strain rate effects. To this end, tensile specimens have been prepared by selective laser sintering, SLS, with different tip notch radii. Experiments have been carried out over a wide range of strain rates, from those representatives of static conditions in electromechanical machines to Hopkinson bar tests at very high strain rates.

2. Experimental procedure

2.1. Materials

A neat polyamide 12 (PA12) was manufactured from PA2200 EOS powders by Prodintec, in Spain, employing selective laser sintering, SLS, technique and an EOS Formiga P-100 LS machine which uses a CO_2 laser configured with the optimum process parameters, which are contained in Table 1.

Density measurements were performed following the Archimedes methodology using distilled water as the submersion liquid in a Metler Toledo AX205 DeltaRange precision balance with a resolution of ± 0.00001 g. Four replicas were carried out for each material getting the following average value and standard deviation: 0.982 ± 0.005 (g/cm^3) and 0.985 ± 0.005 (g/cm^3) for 0° and 90° orientations, respectively.

2.2. Mechanical characterization

Tensile tests were carried out to determine mechanical properties such as tensile strength and Young's modulus. To carry out both the low and high rate tests with the same geometry, tensile specimens were

Table 1
Manufacturing parameters of SLS PA-12 samples.

Particle diameter	Powder bed temperature	Frame temperature	Layer thickness	Laser power
40 – 90 μm	171.5 °C	135.5 °C	0.2 mm	25 W

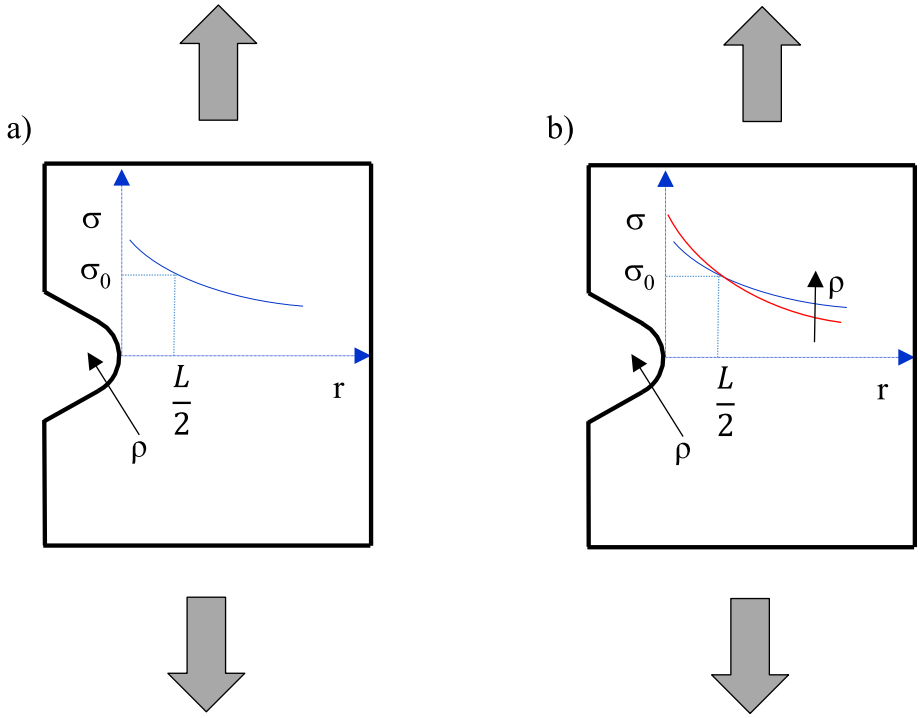

Fig. 1. a) Definition of TCD Point method under mode I loading; b) determination of the critical distance through experimental data with different geometries.

designed to pass from a cylindrical form, with threads for the transmission of load, to a prismatic profile in the central zone, 40 mm in length and a rectangular cross section of 7.5 × 3 mm^2 (Fig. 2). The specimens were prepared both plain and notched. Four different notch radii (0.2, 0.5, 0.8 and 1.0 mm) were used (Fig. 2). The notch was directly created during the SLS manufacturing process. No further machining was applied to these samples as it can lead to some internal damage in the material around notched specimens.

Some additional fracture samples were also prepared with the aim of comparing results from notched and cracked specimens. Due to the layer structure of the samples fabricated by selective laser sintering, which may induce a transversally isotropic mechanical response, two batches of samples with different orientation with respect to the layered structure were tested, one with the load applied parallel to the layered structure (0° orientation) and the other with the load applied perpendicularly (90° orientation).

Low strain rate tests were carried out in a universal electromechanical testing machine MTS Alliance RF/100 equipped with a load cell of ± 5 kN, following the standard ASTM 638–03 (Fig. 3). The crosshead speed was 2 mm/min. Digital image correlation was used for obtaining the displacement field and the longitudinal deformation using a VIC 2D videoextensometer. Because videoextensometry needs reference points to follow their movement during the test, the surface of the specimens was sprayed with black paint to attain a random black pattern of speckles, providing a large quantity of points to be analysed.

The samples for fracture tests were plain tensile samples with a sharp crack generated by sliding a razor blade, previously frozen at liquid nitrogen temperature (-196 °C), till attaining an initial natural crack length of 3 mm and a tip radius at the end of the crack smaller than 10 μm. These values ensure a sharp crack length enough to use the shape factor (equation (3)) to obtain the fracture toughness K_{IC} using Linear Elastic Fracture Mechanics [39]:

$$K_I = F\left(\frac{a}{b}\right)\sigma\sqrt{\pi a} \tag{3}$$

$$F(a/b) = 1.122 - 0.231(a/b) + 10.550(a/b)^2 - 21.710(a/b)^3 + 30.382(a/b)^4$$

Tests at high loading rates were conducted at room temperature, using a split Hopkinson pressure bar (SHPB) in a tensile configuration (Fig. 4). The SPHB device consists of two similar bars (an input and an output bar) with a tensile specimen located between them. Both bars are made of an aluminium alloy, lengths of 2 m for both the input and output bars. The incident bar was a solid bar 12 mm in diameter and the output bar was a hollow bar, with inner radius of 6 mm and outer radius of 12 mm. The projectile, a tube of approximately 1 m length, is impelled against the end of the input bar by means of an air gun. Due to the impact, an elastic tensile pulse is generated in the input bar and travels along it up to the specimen, where is partially reflected and partially transmitted to the output bar (Fig. 5). The amount of reflected and transmitted wave depends on the impedance difference of the bars and the specimen. In the case of the aluminium bars, the impedance is quite higher than in the case of the polymer specimen. This was the reason to use a hollow bar as output bar. The results showed the transmitted wave has been good enough to measure it and the geometry of a hollow bar does not introduce any relevant distortion in the stress wave propagation.

To measure the incident, reflected and transmitted pulses, a full Wheatstone bridge of strain gauges (VISHAY N2A-13-T004K-350) are attached to the bars. The strain gauges signals are recorded using a VISHAY 2200 conditioner connected to a TEKTRONIX TDS 420A digital oscilloscope. In the input bar, two measurement stations were used to work with longer incident waves. The geometry of the dynamic specimens was identical to that of the static tests. Displacements and deformations in the sample were measured by videoextensometry, in a similar way than in static tests, but using a Photrom SA5 high speed camera, capturing images at 300,000 frames per second. The lighting system consists of two lamps avoiding shadows in the image taken. For the determination of Youngs modulus, some gauges were glued in the plain specimens tested in order to measure more accurately the strain in the elastic regime of deformation.

2.3. Finite element modeling

Finite elements analysis was necessary to determine the elastic stress fields needed to apply the TCD, thus, ANSYS and LS-DYNA software have been used to model static and dynamic tests, respectively.

A three-dimensional numerical model including only the specimen has been employed (Fig. 6), imposing the experimental velocities coming from the strain gauges measurement as boundary conditions at both ends of the specimen. The geometry of the test allows the simplification of the model by using two planes of symmetry: one plane defined by the parallel to one side of the rectangular cross-section and containing the longitudinal axe of the sample, and the other symmetry plane defined by the other side of the cross section and the longitudinal axe of the sample. Even more, in static modeling, another symmetry plane defined by a plane perpendicular to the notch and passing through the center of the specimen could be used, finally reducing the static model to 1/8 of the real geometry. This simplification allows to decrease the number of nodes and elements that will compose the finite element mesh, reducing the total number of degrees of freedom in the simulation and hence the associated computational cost.

A mesh formed by 10 node tetrahedral elements (with reduced integration for dynamic simulations) has been considered. In the volume closest to the end of the notch, due to the high stress gradients near the tip, it is necessary to increase the number of elements, so the mesh has been concentrated in that area. The material constitutive equation

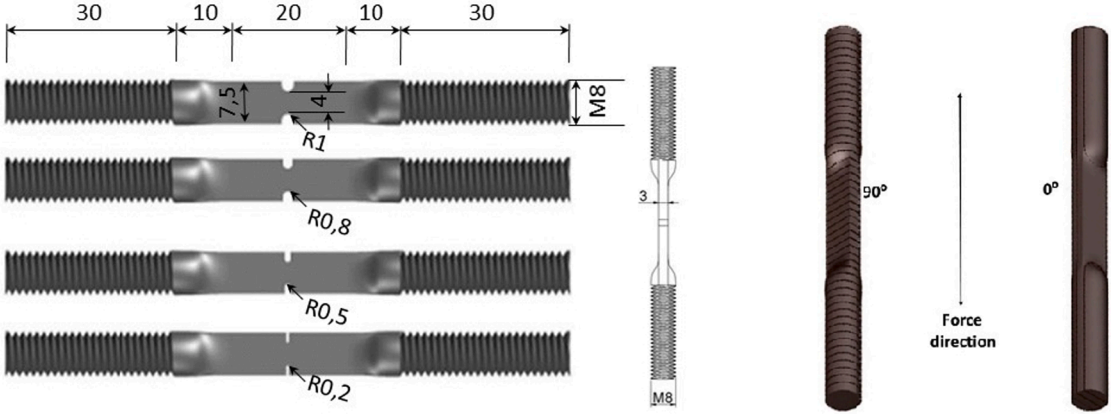

Fig. 2. Notched tensile samples, showing the dimensions and the different tip radii (left) and tensile specimens oriented at 0° and at 90° (right).

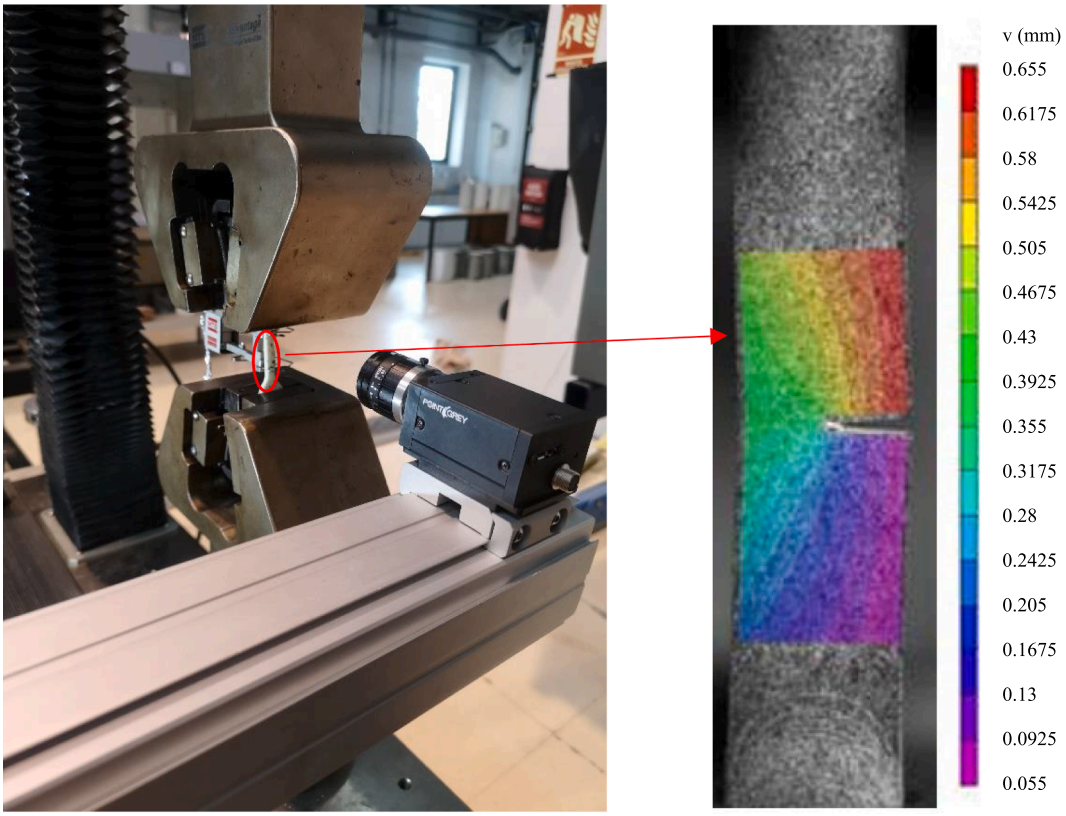

Fig. 3. MTS Alliance RF/100 with the tensile grips installed for the fracture testss at room temperature with the VIC 2D videoextensometer. The cracked sample is painted with a random dot pattern for the digital image correlation (DIC) analysis.

corresponds to a linear elastic behavior with properties taken from the experiments. The stress field around the notch has been determined numerically at the failure instant, to apply the TCD. As brittle behavior is assumed, failure load is considered as the maximum of the force–displacement curves in static tests. In dynamic tests, as the equilibrium was not assured, the failure load was determined with the help of the images from the high speed videoextensometer, when the crack starts to propagate (Fig. 7).

2.4. Weibull statistics

The presence of defects in materials processed by additive manufacturing techniques suggests the use of a probabilistic analysis of the failure loads. In this work, a Weibull distribution has been chosen for simplicity and because it has been widely used with good results. The expression used in this work corresponds to a Weibull distribution with three parameters. The cumulative failure probability (P_{fail}) on which the distribution curve is based, follows the next equation [40–41]:

$$P_{fail}(K_I) = 1 - exp\left[-\left(\frac{K_I - K_{min}}{K_{I0} - K_{min}} \right) \right]^m \quad (4)$$

where K_I is the stress intensity factor in mode I, K_{I0} is a scale parameter located at the 63.2% cumulative failure probability level, m is the shape factor (Weibull modulus), and K_{min} is the lowest stress intensity factor that would cause failure in this kind of samples, that is, a threshold fracture toughness.

3. Results and discussion

3.1. Mechanical characterization

Table 2 summarizes the results from tensile tests and Fig. 8 shows characteristic engineering stress–strain curves of SLS PA 12 at 0° and 90° orientations, obtained from tensile tests at loading rates of 2 mm/min and 500,000 mm/min.

Stress–strain curves at low strain rates shows nonlinear behaviour. At high strain rates the nonlinearity is much less. When this type of behaviour is observed some researchers have proposed the use of an equivalent material model, assuming a linear elastic material with the same energy density as the real one. [42]. This model has not been used in this work. Nevertheless, the group of methodologies under the name of TCD have proved a very good accuracy to predict fracture in notched components, even in the presence of large plasticity.

As can be seen, there is a significant influence on the tensile properties of both the orientation of the samples and the strain rate. In the 0° orientation, the modulus of elasticity is 1.7 GPa at low strain rate, experiencing a dramatic increase of more than 300% in the Hopkinson Bar tests with mean values of 4.2 GPa. These results have been obtained with experiments in which the specimens were instrumented with strain gauges in their central area. The specimens with a 90° orientation exhibited values very similar to those of 0°, both in low and high strain rate tests. It should be clarified at this point that the strain rate shown in Fig. 8 is an estimate corresponding to plain specimens, since in the case of notched samples the strain state is not homogeneous and there is no characteristic strain rate of the specimen. In any case, the loading rates values have been given above.

Yield stress is also influenced by strain rate and orientation. The influence of strain rate is significant, although much less than in the case of Young's modulus. The increases in tensile strength are of the order of 25% in the case of the 90° orientation and 45% for the 0° orientation. The orientation perpendicular to the application of the loads always provides clearly lower tensile strength values, which may be closely related to the presence of defects located between layers due to poor adhesion or non-melted material.

Anisotropy has not been studied in this work beyond testing the

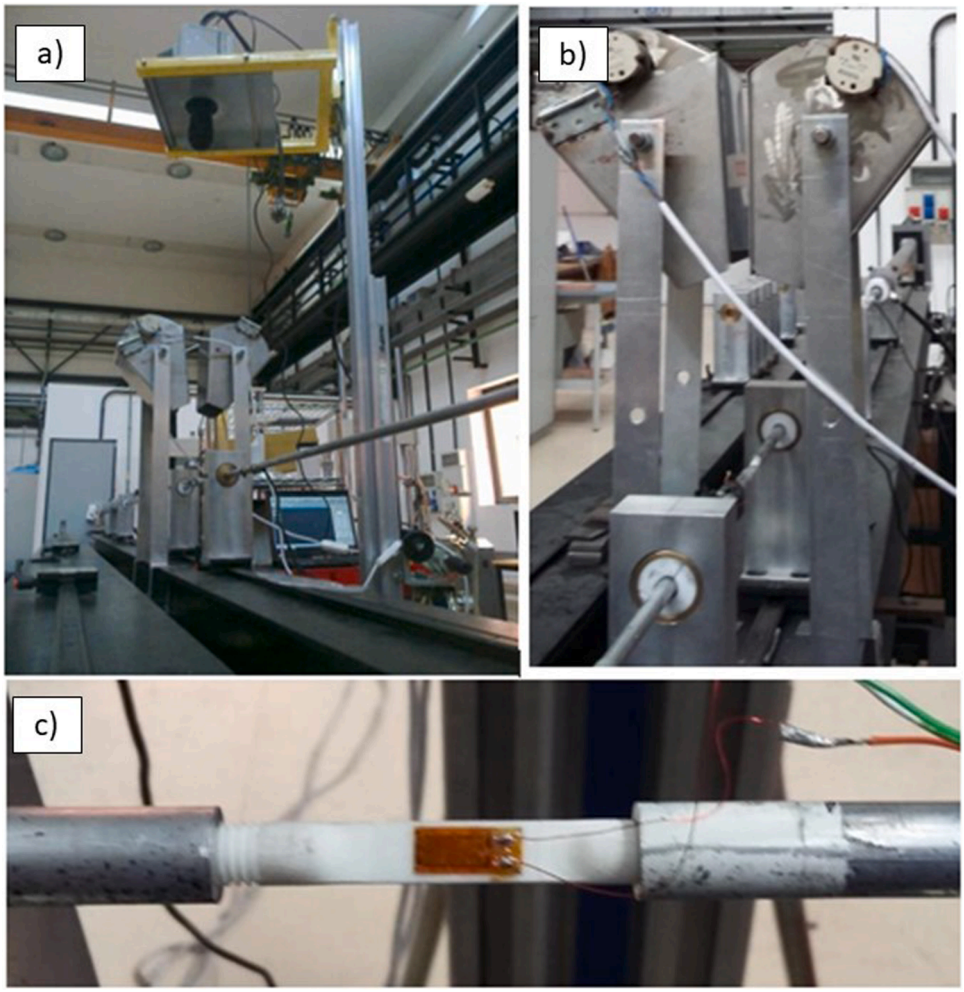

Fig. 4. a) Tensile Hopkinson Bar device for the dynamic tests with the high-speed camera and light system installed; b) detail of both bars in the Hopkinson bar device with the sample between them; c) detail of a tensile sample with a strain gage glued to its surface.

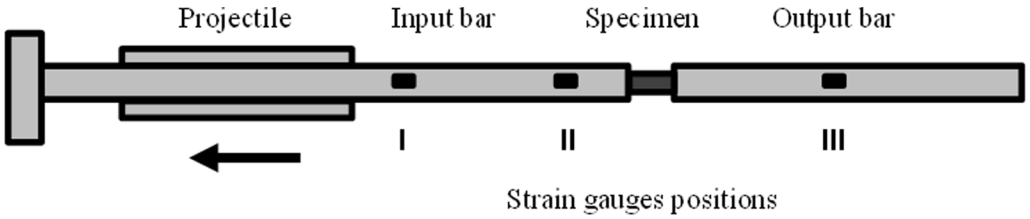

Fig. 5. Schematic representation of the SHPB setup.

material in different orientations. Some examples of considering anisotropic behavior can be found in the literature [43].

3.2. Notched and cracked specimens

In order to make predictions of fracture toughness of SLS PA 12 from notched specimens, the material parameters of the TCD have been calibrated through a combination of fracture tests on notched specimens and finite elements simulations. The notch fracture toughness (K_{IC}^{N}), which is obtained by the application of Creager and Paris equation for linear elastic stress field [44] has been calculated from the next equation:

$$K_{IC}^{N}(\rho,t)=\frac{\sigma_{tip}(\rho,t)}{2}\sqrt{\pi\rho}=k_t(\rho,t)\frac{F_{max}(\rho,t)}{2A_0}\sqrt{\pi\rho} \quad (5)$$

where σ_{tip} is the stress at the tip of the notch, ρ is the notch radius of each sample measured using a profile projector, $k_t(\rho,t)$ is the stress concentration factor for each tip radius, F_{max} is the corresponding maximum load and A_0 is the nominal specimen cross section. In dynamic tests, the tip stress, maximum load and stress concentration factor depend on time as waves are travelling inside the specimen and equilibrium is not necessarily assured, at least during the first instants of loading.

The evolution of the stress concentration factor with time during a Hopkinson bar test is shown in Fig. 9. It can be observed how after a few microseconds with a lot of oscillations, k_t presents a smooth behaviour during the test. The value used in equation (5) was that indicated in Fig. 9 at the corresponding fracture time.

K_{IC}^{N} results are shown graphically in Fig. 10. The increase in the notch fracture toughness is much more appreciated for dynamic rather than for static conditions. Moreover, for each strain rate, samples with 90°

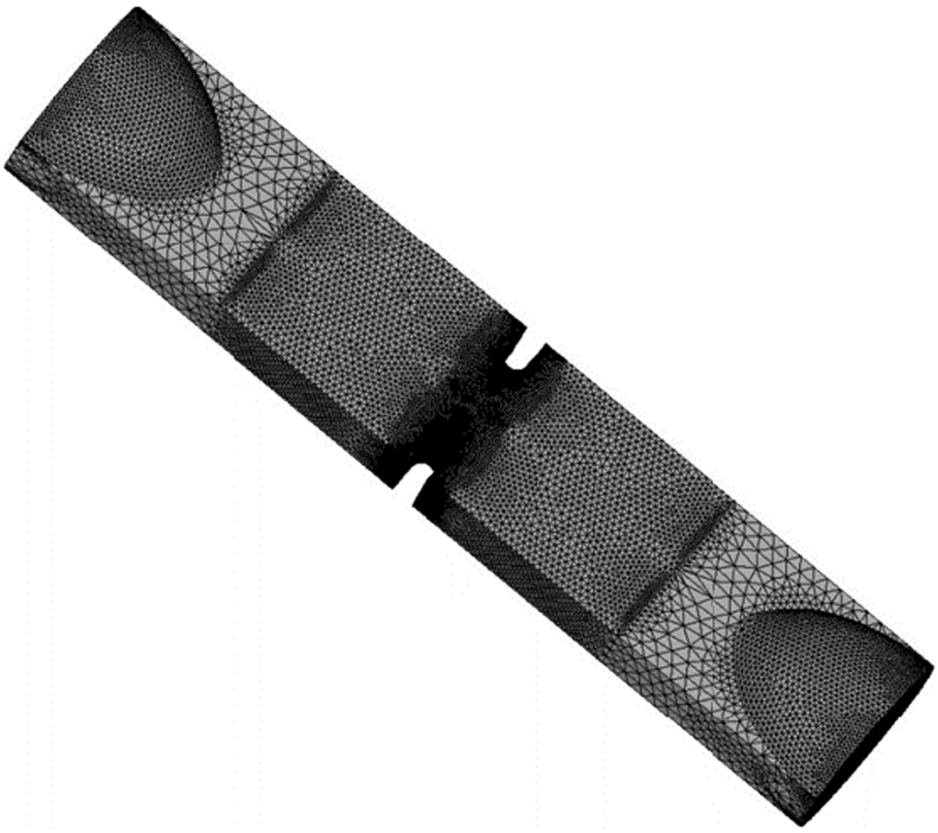

Fig. 6. Full geometry and mesh of the specimens (notch tip radius of 0,5 mm) used in ANSYS and LS-Dyna. Only one quarter was modelled due to symmetry.

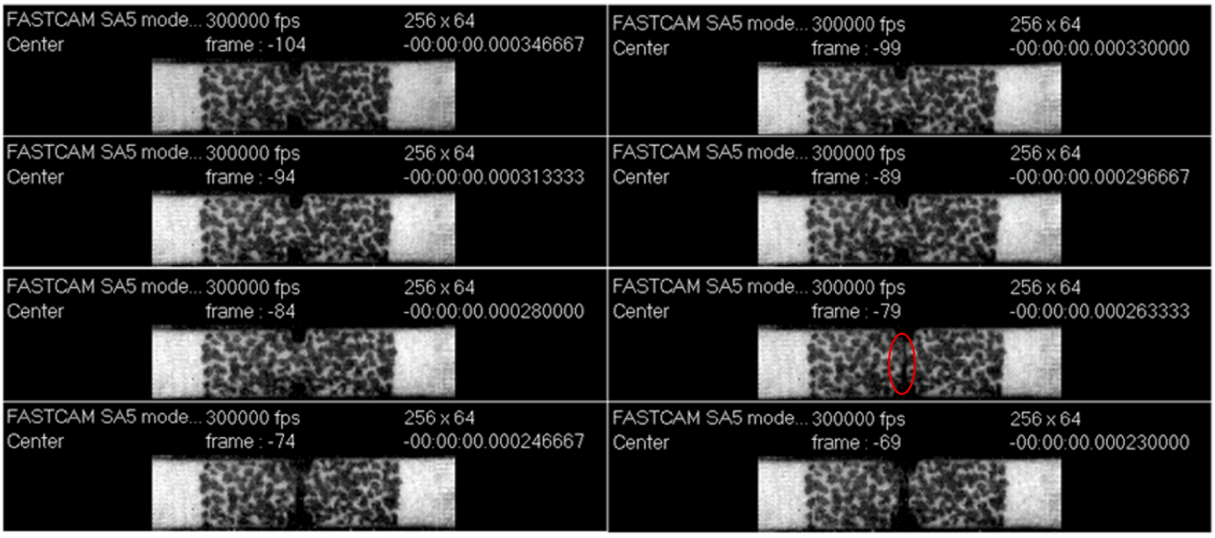

Fig. 7. Example of the high speed camera images captured at 300,000 fps, showing the pattern defined in the sample and the start of the crack growing after 83 microseconds from the start of the tests.

Table 2
Evolution of the Young's modulus and tensile strength with strain rate in SLS PA12 at 0° and 90° orientations.

		0° orientation	90° orientation
Low strain rate (10^{-3} s^{-1})	Tensile strength (MPa)	49 ± 2	34 ± 12
	Young's modulus (GPa)	1.7 ± 0.1	1.6 ± 0.1
High strain rate (500–600 s^{-1})	Tensile strength (MPa)	72 ± 4	43 ± 11
	Young's modulus (GPa)	4.2 ± 0.2	4.0 ± 0.1

orientation present higher scatter and lower values of K_{IC}^{N} than those observed in 0° oriented samples.

3.3. Application of the TCD

Finite element simulations were performed assuming a liner elastic behaviour to determine the notch tip stress field at failure. The stress-distance curve was obtained at the central notch section, as shown in Figs. 11 and 12. The failure load used to calculate these curves was the

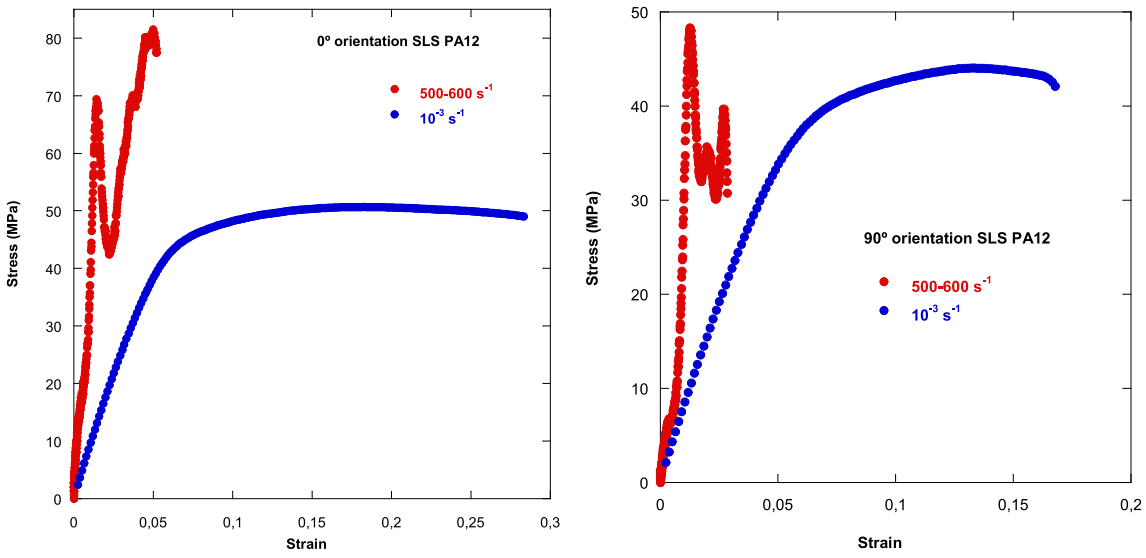

Fig. 8. Engineering stress–strain curves with 0° and 90° orientation at low and high strain rates.

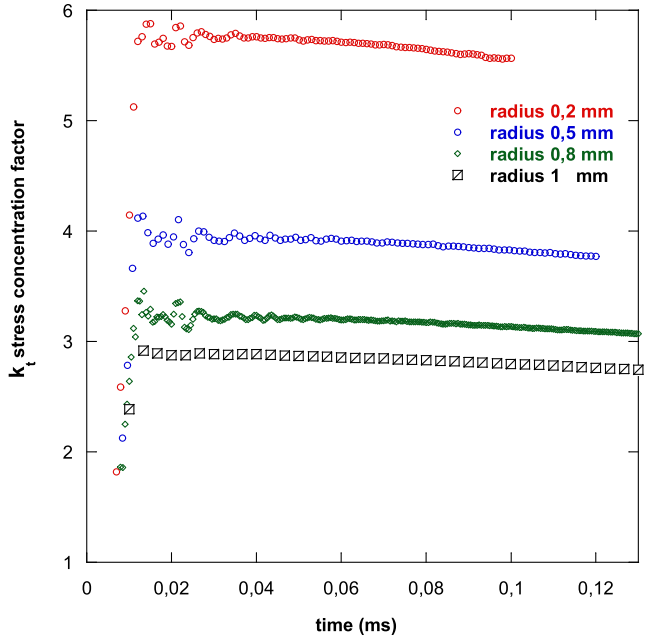

Fig. 9. Stress concentration factor vs. time during a Hopkinson bar test, for the four different notch tip radii studied.

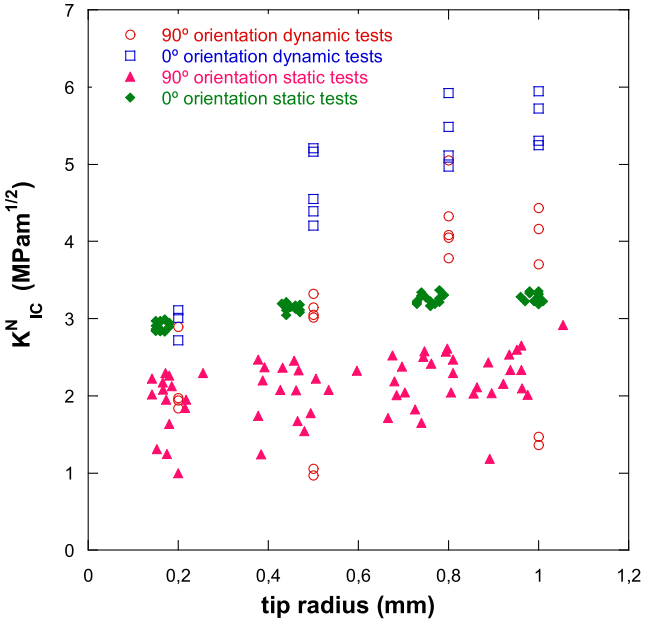

Fig. 10. Apparent fracture toughness for the different tip notch radii.

average of the different tests that make up a set of samples (each set is characterized by a nominal notch tip radius, orientation, and strain rate). When applying the TCD to different geometries through the Point Method (PM), the appearance of multiple intersection points may arise. To overcome this problem, only the stress-distance curves for the highest and lowest notch tip radius were used to determine the TCD parameters. Table 3 and Figs. 11 and 12 show the corresponding results, providing, the σ_0 and L values obtained for both manufactured orientations and strain rates. A first value for the fracture toughness was obtained using directly the TCD parameters.

Moreover, the TCD provides expressions that allow the fracture toughness to be calculated based on the notch fracture toughness (K_{IC}^N) obtained from notched components. Among the different versions of the TCD, if the PM is considered the given equation is:

$$K_{IC} = K_{IC}^N \frac{\left(1+\frac{2\rho}{L}\right)}{\left(1+\frac{\rho}{L}\right)^{3/2}} \tag{6}$$

Fracture toughness values (critical values of the stress intensity factor) obtained for each orientation were fitted by a Weibull distribution function. For static tests, each set of samples with different notch tip radii were adjusted with a different Weibull distribution, as a good number of consistent data were available, and one distribution was obtained considering all the radii together. For dynamic tests, all the different notch radii were analysed at the same time. The final Weibull probability distribution equations for all the tip notch radii together are presented in Table 4 for both orientations and strain rates.

Fig. 13 shows the cumulative probability, P_{fail}, versus mode I stress intensity factor for each orientation and strain rate. Although the individual Weibull distributions associated with each notch tip radius have not been included for brevity, the distribution parameters are similar to

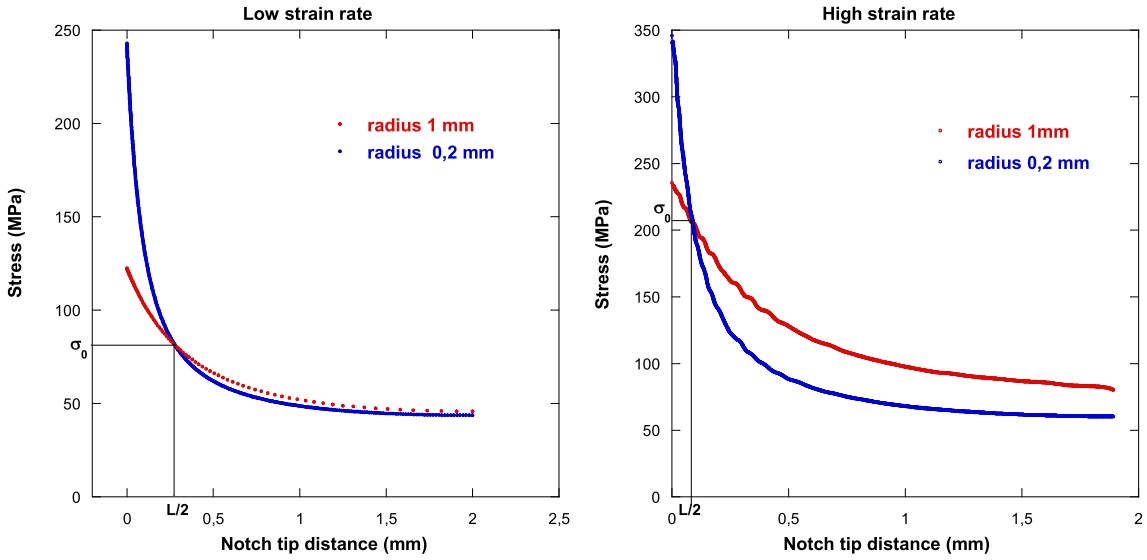

Fig. 11. Stress–distance curves corresponding to extreme notch tip radii (the highest tip radii, 1 mm and the lowest, 0.2 mm) of 0° orientation samples: low strain rate (left) and high strain rate (right).

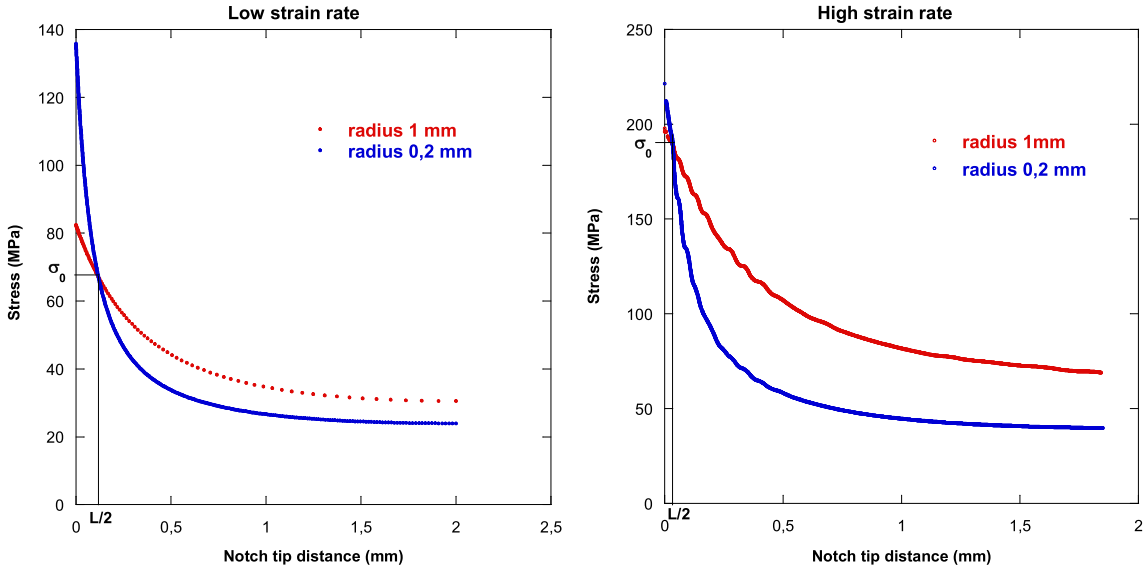

Fig. 12. Stress–distance curves corresponding to extreme notch tip radii (the highest tip radii, 1 mm and the lowest, 0.2 mm) of 90° orientation samples: low strain rate (left) and high strain rate (right).

Table 3
TCD parameter values versus strain rate and orientation.

	SLS PA12 0° orientation			SLS PA12 90° orientation		
strain rate	σ_0(MPa)	L(μm)	$K_{IC}^{TCD} = \sigma_0\sqrt{\pi L}$(MPa·m$^{1/2}$)	σ_0(MPa)	L(μm)	$K_{IC}^{TCD} = \sigma_0\sqrt{\pi L}$(MPa·m$^{1/2}$)
10^{-3} s^{-1}	81	560	3.4	67	236	1.8
≈550 s^{-1}	205	180	4.9	180	80	2.9

those of the distribution obtained by considering all the radii together, which is a sign of the consistency of the procedure used.

The fracture toughness was also calculated from cracked specimen using the Linear Elastic Fracture Mechanics (equation (3)). After probabilistic analysis using a Weibull distribution, results are compiled in Table 5, where a comparison of dynamic and static K_{I0} values (63.2% failure probability) for cracked and notched samples is presented.

Table 4
Weibull statistical distributions from the total number of notched specimens tested at low and high strain rates.

Low strain rate	
0° orientation	**90° orientation**
$P_{fail}(K_{IC}) = 1 - exp\left[-\left(\frac{K_{IC} - 2.90}{3.31 - 2.90}\right)\right]^{3.35}$	$P_{fail}(K_{IC}) = 1 - exp\left[-\left(\frac{K_{IC}}{2.10}\right)\right]^{6.23}$
High strain rate	
0° orientation	**90° orientation**
$P_{fail}(K_{IC}) = 1 - exp\left[-\left(\frac{K_{IC} - 0.20}{4.26 - 0.20}\right)\right]^{8.37}$	$P_{fail}(K_{IC}) = 1 - exp\left[-\left(\frac{K_{IC} - 1.47}{2.31 - 1.47}\right)\right]^{2.42}$

specimens at low strain rates are 41% and reach more than 120% at high strain rates.

Comparing the fracture toughness values in Table 3 and Table 5, the TCD appears to be adequate for calculating the actual fracture toughness from notched samples of the SLS PA12 material at low strain rates, showing only a deviation of 3% in the case of 0° orientation and 17% in the case of 90° orientation. This effect is probably due to the presence of manufacturing defects and lack of adhesion between the layers that weakens the sample in this direction. However, at high strain rates, this methodology acceptably predicts the fracture toughness value only in the case of 0° orientation. The TCD prediction in a 90° orientation is much lower than that obtained from cracked specimens.

Finally, it is relevant to discuss the question of equilibrium conditions in dynamic tests. At low loading rates, equilibrium is assured during the whole test and the validity of the Creager and Paris equation is basically correct. However, under dynamic conditions the propagation of stress waves must be considered. Fig. 14 shows the forces at both

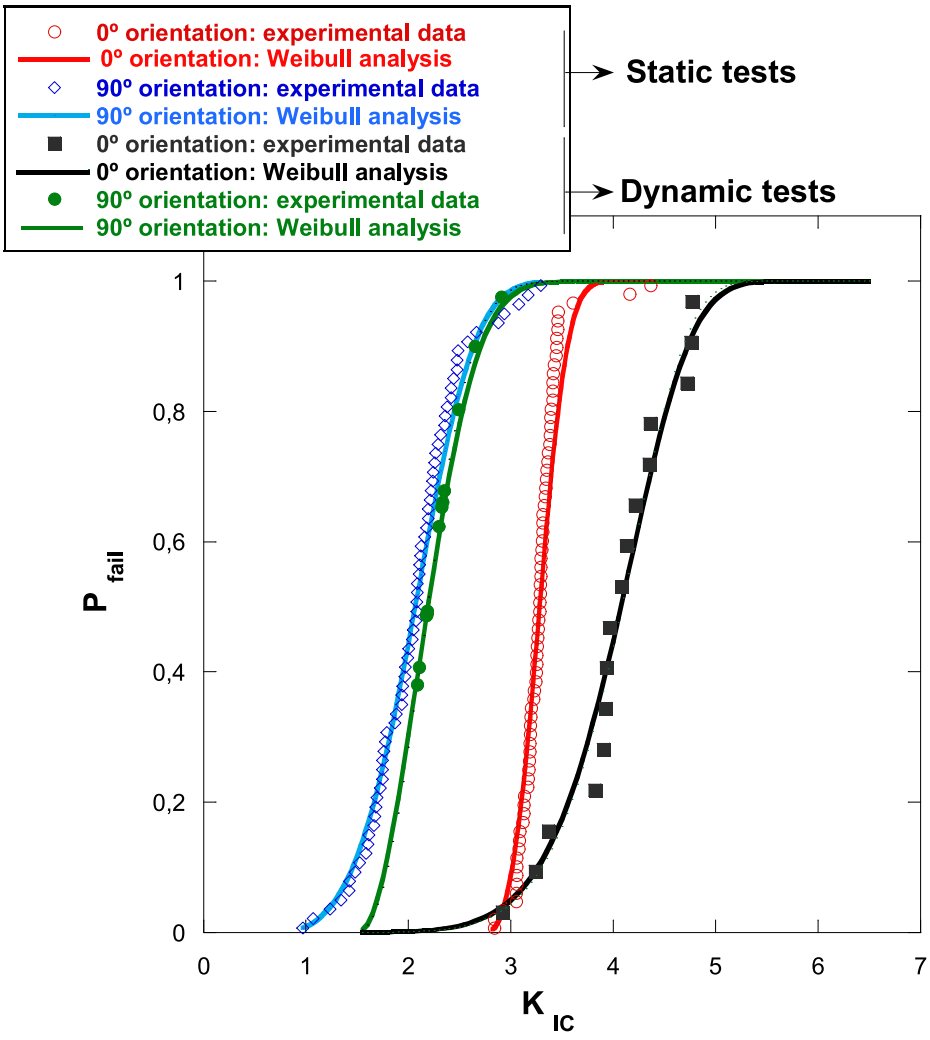

Fig. 13. Comparison of Weibull distributions and experimental data for each specimen orientation and strain rate.

Considering the values of stress intensity factor that give a failure probability of 63.2%, K_{I0}, the agreement between notched and cracked specimens with 0° orientation is really good at low strain rates, and it is also quite acceptable even at higher strain rates, showing differences of only 13%, being lower when calculated from notched specimens. The situation is not the same in the case of the 90° orientation since the differences between the results provided by the notched and cracked ends of the specimen (the impact face is in contact with the incident bar and the output face is attached to the transmitting bar) and at the central section where the notch has been made. As can be seen, the forces are not so different, although the differences may be relevant at some moments. Fig. 15 shows an example of the stress-distance curves obtained in the vicinity of the notch tip in the LS-DYNA numerical simulation of a Hopkinson bar test at the failure time and the comparison with those

Table 5
Comparison of dynamic and static K_{I0} values (63.2% samples under analysis will have failed/failure probability) for cracked and notched samples.

	SLS 0° orientation		SLS 90° orientation	
strain rate	Sample notch radius (mm)	K_{I0}(MPa·m$^{1/2}$)	Sample notch radius (mm)	K_{I0}(MPa·m$^{1/2}$)
10^{-3} s^{-1}	0.2	3.13	0.2	2.24
	0.5	3.41	0.5	2.14
	0.8	3.35	0.8	2.01
	1	3.25	1	2.00
	All radii	3.31	All radii	2.10
	Cracked	3.39	Cracked	2.96
≈550 s^{-1}	All radii	4.26	All radii	2.31
	Cracked	4.834	Cracked	5.09

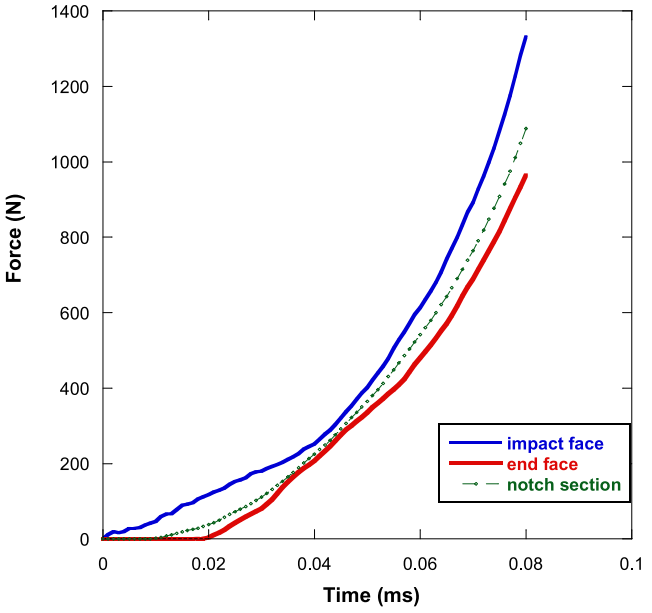

Fig. 14. Forces calculated from the LS-DYNA simulation of a Hopkinson bar tests, at both ends of the sample and in the middle, where the notch tip is located.

corresponding to the elastic stress fields associated with the Creager and Paris equation. The good approximation in the area near the tip is sufficient to validate the use of the Creager and Paris equation also at high loading rates.

4. Conclusions

In this work, the applicability of the TCD to characterize the behavior of polyamide 12 notched specimens at high strain rates has been evaluated and the fracture toughness has been quantified in different orientations of the material in static and dynamic tests. The experiments and the numerical simulation carried out allow the following conclusions to be drawn:

- A numerical-experimental methodology based on the TCD has been developed to characterize the behavior of notched polyamide 12 specimens under static and dynamic conditions. The results obtained allow us to affirm that the TDC can provide acceptable results also at high strain rates.
- The effects of the orientation of the specimens in relation to the direction of deposition have been studied, obtaining properties in orientations parallel and perpendicular to the layers of deposited material. The anisotropic character of the material has been quantified in the modulus of elasticity, in the tensile strength and in the fracture toughness. The values in the specimens oriented perpendicular to the layers of material are usually lower than those obtained in specimens oriented parallel, especially at high strain rates.
- The direct use of the critical stress σ_0 and the characteristic length L as TCD parameters provides a simple and reasonable estimation of the fracture toughness in all the cases studied, except for the specimens oriented perpendicular to the layers and tested at high temperatures. strain rate.

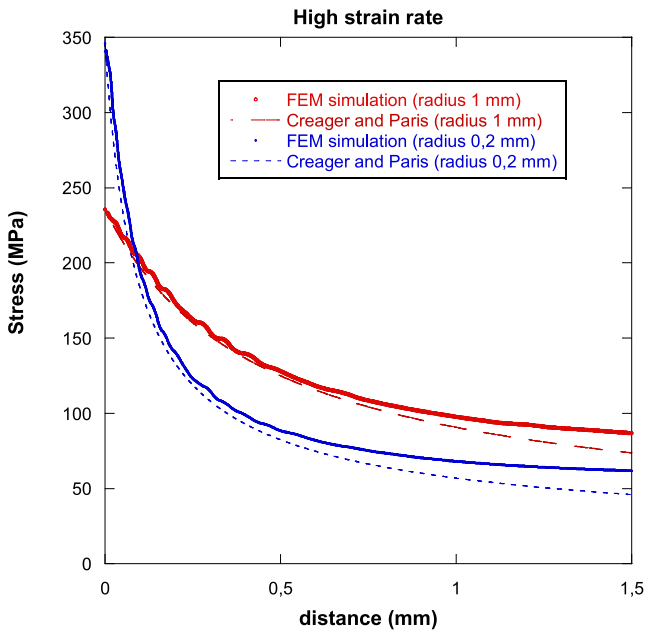

Fig. 15. Creager and Paris linear stress field around a notch tip and stress fields calculated from LS-DYNA simulations at failure time for 90° orientation samples with tip radius 1 mm and 0,2 mm.

CRediT authorship contribution statement

T. Gómez-del Río: Conceptualization, Methodology, Investigation, Writing – original draft. **M. Crespo:** Conceptualization, Methodology, Investigation. **R. López:** Conceptualization, Methodology. **J. Rodríguez:** Conceptualization, Investigation, Supervision, Writing – review & editing, Funding acquisition.

Declaration of Competing Interest

The authors declare that they have no known competing financial interests or personal relationships that could have appeared to influence the work reported in this paper.

Acknowledgement

Authors are indebted to Ministerio de Ciencia e Innovación of Spain for their financial support through grant PID2019-108968RB-I00.

References

[1] A.S. Argon (Ed.), The Physics of Deformation and Fracture of Polymers, Cambridge University Press, 2013.
[2] J. Richeton, S. Ahzi, L. Daridon, Y.A. Rémond, Formulation of the cooperative model for the yield stress of amorphous polymers for a wide range of strain rates and temperatures, Polymer 46 (2005) 6035–6043, https://doi.org/10.1016/j.polymer.2005.05.079.

[3] T. Gómez-del Río, J. Rodríguez, Compression yielding of polypropylenes above glass transition temperature, Eur. Polym. J. 46 (6) (2010) 1244–1250.
[4] D.A. Serban, G. Weber, L. Marsavina, V.V. Silberschmidt, W. Hufenbach, Tensile properties of semi-crystalline thermoplastic polymers: Effects of temperature and strain rates, Polym. Test. 32 (2013) 413–425. https//doi.org/ 10.1016/j.polymertesting.2012.12.002.
[5] C.P. Buckley, P.J. Dooling, J. Harding, C. Ruiz, Deformation of thermosetting resins at impact rates of strain. Part 2: Constitutive model, J. Mech. Phys. Sol. 52 (2004) 2355–2377. https//doi.org/ 10.1016/j.jmps.2004.04.001.
[6] T. Gómez-del Río, J. Rodríguez. Compression yielding of epoxy: Strain rate and temperature effect, Mater. Des. 35 (2012) 369–373. https//doi.org/ 10.1016/j.matdes.2011.09.034.
[7] H. Eyring, Viscosity, Plasticity, and Diffusion as Examples of Absolute Reaction Rates, J. Chem. Phys. 4 (1936) 283–291. https//doi.org/.
[8] C. Bauwens-Crowet, J.C. Bauwens, G. Homès, Tensile yield-stress behavior of glassy polymers, J. Polym. Sci. A 2 (7) (1969) 735–742, https://doi.org/10.1063/1.1749836.
[9] R.D. Goodridge, C.J. Tuck, R.J.M. Hague, Laser sintering of polyamides and other polymers, Prog. Mater Sci. 57 (2) (2012) 229–267.
[10] M. Bhuvanesh Kumar, P. Sathiya, Methods and materials for additive manufacturing: A critical review on advancements and challenges, Thin-Walled Struct. 159 (2021), 107228, https://doi.org/10.1016/j.tws.2020.107228.
[11] K. Narsimlu, A.G. Pathak, A.G. Mulky, C. Yavarna, A Market Analysis on impact of additive layer manufacturing technologies on aerospace and defense supply chain, Int. J. Manag. 8 (2) (2017) 171–187.
[12] A. Forster. Materials testing standards for additive manufacturing of polymer materials: state of the art and standards applicability. National Institute of Standards and Technology Interagency Report 8059. 2015.
[13] S.A.M. Tofail, E.P. Koumoulus, A. Bandyopadhyay, S. Bose, L. O'Donoghue, C. Charitidis, Additive manufacturing: scientific and technological challenges, market uptake and opportunities, Mater. Today 21 (1) (2018) 22–37, https://doi.org/10.1016/j.mattod.2017.07.001.
[14] R.D. Goodridge, R.J.M. Hague, C.J. Tuck, Effect of long-term ageing on the tensile properties of a polyamide 12 laser sintering material, Polym. Test. 29 (4) (2010) 483–493, https://doi.org/10.1016/j.polymertesting.2010.02.009.
[15] B. Caulfield, P.E. McHugh, S. Lohfeld, Dependence of mechanical properties of polyamide components on build parameters in the SLS process, J. Mater. Process. Technol. 182 (1–3) (2007) 477–488, https://doi.org/10.1016/j.jmatprotec.2006.09.007.
[16] T. Stichel, T. Frick, T. Laumer, F. Tenner, T. Hausotte, M. Merklein, M. Schmidt, A Round Robin study for Selective Laser Sintering of polyamide 12: Microstructural origin of the mechanical properties, Opt. Laser Technol. 89 (2017) 31–40.
[17] T.L. Starr, T.J. Gornet, J.S. Usher, The effect of process conditions on mechanical properties of laser-sintered nylon, Rapid Prototyp. J. 17 (6) (2011) 418–423, https://doi.org/10.1108/13552541111184143.
[18] J. Schneider, S. Kumar, Multiscale characterization and constitutive parameters identification of polyamide (PA12) processed via selective laser sintering, 2019, p. 106357, Polym. Test. 86 (December) (2020), https://doi.org/10.1016/j.polymertesting.2020.106357.
[19] D.I. Stoia, L. Marşavina, E. Linul, Correlations between Process Parameters and Outcome Properties of Laser-Sintered Polyamide, Polymers (Basel) 11 (11) (Nov. 2019) 1850, https://doi.org/10.3390/polym11111850.
[20] R. Seltzer, F.M. de la Escalera, J. Segurado, Effect of water conditioning on the fracture behavior of PA12 composites processed by selective laser sintering, Mater. Sci. Eng. A 528 (22–23) (2011) 6927–6933, https://doi.org/10.1016/j.msea.2011.05.045.
[21] D.J. Hitt, B. Haworth, N. Hopkinson, Fracture mechanics approach to compare laser sintered parts and injection mouldings of nylon-12, Proc. Inst. Mech. Eng. Part B J. Eng. Manuf. 225 (9) (2011) 1663–1672, https://doi.org/10.1177/0954405411402141.
[22] E. Linul, L. Marsavina and D. I. Stoia, "Mode I and II fracture toughness investigation of Laser-Sintered Polyamide," Theor. Appl. Fract. Mech., vol. 106, no. December 2019, p. 102497, 2020, doi: 10.1016/j.tafmec.2020.102497.
[23] H. Neuber, Theory of notch stresses: principles for exact calculation of strength with reference to structural form and material, Springer Verlag, Berlin, 1958.
[24] P. Lazzarin, R. Tovo, A unified approach to the evaluation of linear elastic stress fields in the neighbourhood of cracks and notches, Int. J. Fract. 78 (1996) 3–19.
[25] S. Filippi, P. Lazzarin, R. Tovo, Developments of some explicit formulas useful to describe elastic stress fields ahead of notches in plates, Int. J. Solids Struct. 39 (17) (2002) 4543–4565.
[26] F. Berto, P. Lazzarin, Recent developments in brittle and quasi-brittle failure assessment of engineering materials by means of local approaches, Mater. Sci. Engng, R 75 (2014) 1–48.
[27] G. Glinka, Calculation of inelastic notch-tip strain-stress histories under cyclic loading, Engng. Fract. Mech. 22 (5) (1985) 839–854, https://doi.org/10.1016/0013-7944(85)90112-2.
[28] F.J. Gomez, G.V. Guinea, M. Elices, Failure criteria for linear elastic materials with U-notches, Int. J. Fract. 2006 (141) (2006) 99–113.
[29] D. Taylor, The theory of critical distances: a new perspective in fracture mechanics, Elsevier, 2007.
[30] D. Taylor, M. Merlo, R. Pegley, M.P. Cavatorta, The effect of stress concentrations on the fracture strength of polymethylmethacrylate, Mater. Sci. Engng. 382 (2004) 288–294, https://doi.org/10.1016/j.msea.2004.05.012.
[31] M.R. Ayatollahi, A.R. Torabi, Brittle fracture in rounded-tip V-shaped notches, Mater. Des. 31 (1) (2010) 60–67, https://doi.org/10.1016/j.matdes.2009.07.017.
[32] S. Cicero, V. Madrazo, I.A. Carrascal. Analysis of notch effect in PMMA using the Theory of Critical Distances. Engng. Fract. Mech. 86 (2012) 56–72. https://doi.org/ 10.1016/j.engfracmech.2012.02.015.
[33] L. Susmel, D. Taylor, A novel formulation of the theory of critical distances to estimate lifetime of notched components in the medium-cycle fatigue regime, Fatigue Fract. Eng. Mater. Struct. 30 (7) (2007) 567–581.
[34] L. Susmel, D. Taylor, On the use of the Theory of Critical Distances to predict static failures in ductile metallic materials containing different geometrical features, Eng. Fract. Mech. 75 (15) (2008) 4410–4421.
[35] L. Susmel, D. Taylor, The theory of critical distances to predict static strength of notched brittle components subjected to mixed-mode loading, Eng. Fract. Mech. 75 (3-4) (2008) 534–550.
[36] A.J. Kinloch, J.G. Williams, Crack blunting mechanism in polymers, J. Mater. Sci. 15 (1980) 987–996.
[37] T. Yin, A. Tyas, O. Plekhov, A. Terekhina, L. Susmel, A novel reformulation of the Theory of Critical Distances to design notched metals against dynamic loading, Mater. Design 69 (2015) 197–212, https://doi.org/10.1016/j.matdes.2014.12.026.
[38] M. Crespo, M.T. Gómez-del Río, J. Rodríguez, Failure of SLS polyamide 12 notched samples at high loading rates, Theor. Appl. Fract. Mech. 92 (2017) 233–239.
[39] H. Tada, P. Paris y G. Irwin, The Stress Analysis of Cracks Handbook, Ney York: The American Society of Mechanical Engineers (ASME-Press), 2000.
[40] H. Rinne, The Weibull distribution: a handbook, CRC Press, Boca Raton, FL, 2009.
[41] W. Weibull, A statistical distribution function of wide applicability, ASME J. Appl. Mech. 18 (1951) 293–297, https://doi.org/10.1115/1.4010337.
[42] A.R. Torabi, Estimation of tensile load-bearing capacity of ductile metallic materials weakened by a V-notch: The equivalent material concept, Mat. Sci. Eng. A. 536 (2012) 249–255, https://doi.org/10.1016/j.msea.2012.01.007.
[43] A.R. Torabi, E. Pirhadi, Notch failure in laminated composites under opening mode: The Virtual Isotropic Material Concept, Compos. Part B: Eng. 172 (2019) 61–75.
[44] M. Creager, C. Paris, Elastic field equations for blunt cracks with reference to stress corrosion cracking, Int. J. Fract. 3 (1967) 247–252, https://doi.org/10.1007/BF00182890.